

Bond of reinforcement in self-compacting steel-fibre reinforced concrete  
Anette Jansson, Ingemar Löfgren, Karin Lundgren and Kent Gylltoft

Published in Magazine of Concrete Research, see journal homepage  
<http://www.icevirtuallibrary.com/content/journals>

"Permission is granted by ICE Publishing to print one copy for personal use. Any other use of these PDF files is subject to reprint fees."

# Bond of reinforcement in self-compacting steel-fibre-reinforced concrete

**Anette Jansson**

PhD student, Chalmers University of Technology, Göteborg, Sweden

**Ingemar Lofgren**

PhD student, Chalmers University of Technology, Göteborg, Sweden

**Karin Lundgren**

Associate Professor, Chalmers University of Technology, Göteborg, Sweden

**Kent Gylltoft**

Professor, Chalmers University of Technology, Göteborg, Sweden

Crack control, one of the main benefits of using fibre reinforcement, depends to a large extent on the concrete-rebar bond. Pull-out tests of specimens with short embedment length were carried out and the results showed no effect from the fibres on the normalised bond-slip behaviour before peak load. After this, the fibre reinforcement provided extra confinement, changing the failure mode from splitting to pull-out failure. The test results were used to calibrate a finite-element bond model that considers both tangential stresses and stresses in the radial direction from the rebar. Splitting cracks may be thus considered in the finite-element analyses. The model proved to yield results in good agreement with the experimental results regarding failure mode, load-slip relation and splitting strains on the surfaces of the pull-out specimens. The analyses revealed that two types of action were active in the cracking process. In addition, the confinement effect of the fibre reinforcement was compared with the confinement of conventional stirrups using the bond model in CEB-FIP model code 2010.

## Introduction

Although it is well known that adding fibres to a matrix will lead to smaller crack widths and increase tension stiffening (Noghabai, 1998) while also reducing the distance between cracks (Bischoff, 2003), there is still a need for better knowledge of the cracking behaviour regarding the small crack widths related to the serviceability state of a structure. Crack control, one of the main benefits of using fibre reinforcement, depends to a large extent on the bond mechanism of the reinforcement bar-matrix system. The pull-out behaviour depends on the characteristics of the reinforcement bar (geometry and steel type), the surrounding matrix (packing grade, and fibre type and amount) and the level of lateral confinement (cover thickness, amount of transverse reinforcement, possible support pressure, etc.). During pull-out, inclined transverse cracks are initiated at the contact points between the steel lugs and concrete, and the bond action generates inclined forces that radiate outwards in the concrete. The inclined stress is often divided into a longitudinal component, called the bond stress, and a radial component, called the normal or splitting stress. The inclined forces are balanced by tensile ring stresses in the surrounding concrete, as explained by Tepfers (1973) (Figure 1). If the tensile stress becomes larger than the tensile strength of the matrix, longitudinal splitting cracks will form in the concrete. Fibre reinforcement will suppress the opening of these cracks and thus provide extra confinement.

Researchers agree that fibre reinforcement improves bond strength in the case of splitting failure. Regarding the effect at

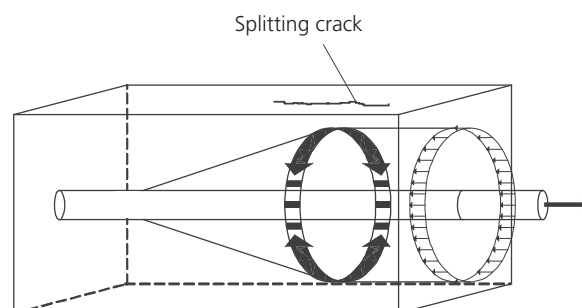


Figure 1. Tensile ring stresses in the anchorage zone according to Tepfers (1973)

pull-out failure and the bond stiffness (pre-peak behaviour), contradictory results have been reported, as concluded in the state-of-the-art report of Bigaj-van Vliet (2001).

Different fibre materials and geometry yield different pull-out behaviour; for example, Chao *et al.* (2009) show that the addition of 1% by volume of the synthetic fibre UHM-PE 38 mm (polyethylene) yielded a markedly higher peak stress and residual stress compared with a matrix reinforced with 1% regular hooked-end steel fibres of 30 mm length. With a diameter of only 0.038 mm, for random three-dimensional (3D) distribution, the average number of synthetic fibres was 400/cm<sup>2</sup> compared with 2/cm<sup>2</sup> for steel fibre of diameter

0.55 mm. The larger number of polyethylene fibres can effectively maintain the early confinement. For larger deformations, the steel fibre, with its higher Young's modulus, became more effective.

Self-compacting concrete (SCC) has been found to improve bond properties of single fibres. Grünwald (2004) reported an increase in fibre pull-out force of 15–50% for SCC in strength class C45/55. The concrete–rebar bond may also gain from the use of SCC. Zhu *et al.* (2004) found that SCC improved the magnitude of the bond stress in pull-out tests. They compared plain non-fibrous vibrated concrete, plain non-fibrous SCC and fibre-reinforced SCC. In their tests, the peak bond strength was increased by the use of SCC compared with plain vibrated concrete, but there was no additional improvement from the addition of fibres (RC 65/35BN 30 kg/m<sup>3</sup>) to the SCC.

The aim of the present study was to obtain relevant bond properties for self-compacting steel-fibre-reinforced concrete (SCSFRC) to steel bars. These properties were then used in finite-element (FE) analyses of the cracking behaviour of reinforced SCSFRC prisms, known as tie elements. To simulate the cracking behaviour of these tie elements with FE analysis, it is necessary to properly describe the interaction between the rebar and the concrete. Owing to the contradictory findings in the literature, it was decided to carry out pull-out tests on specimens with a short embedment length.

The results from the pull-out tests were used to calibrate a bond–slip model developed by Lundgren (2005). This model describes both the tangential and the radial deformation between the rebar and the concrete. Hence, the splitting stresses developing from the inclined compressive struts can also be studied. By combining tests and analyses of this kind, it is possible to study the effect of fibres – both the confining action they provide and their local effect on the rebar–concrete interface.

## Experimental programme

### Materials

#### Concrete mix

The concrete used was self-compacting (slump flow spread 650–780 mm) with a water/cement ratio of between 0.53 and 0.55. The concrete mixes were manufactured at a ready-mix plant in batches of 2 m<sup>3</sup> using a central drum mixer with a capacity of 6 m<sup>3</sup>. Table 1 shows the concrete mix compositions.

#### Fibre washout

To determine the actual fibre content, a washout control was carried out for each of the batches with steel fibres. The washout control was done in accordance with SS-EN 14721: 2005 (SIS, 2005a) and three samples of 8 l each were taken from each batch. As the concrete was poured from the truck, one sample was taken at the beginning, one in the middle and one at the end of the

Series	Content: kg/m <sup>3</sup>				
	0.0	0.25	0.5	1.0a	1.0b
CEM II/A-LL	359	361	362	368	357
Water	197	195	197	202	189
Sand 0–4 mm	679	748	808	693	661
Sand 0–8 mm	231	146	161	160	168
Gravel 5–8 mm	156	122	54	166	183
Gravel 8–16 mm	590	566	554	569	580
Limestone filler	182	207	182	172	182
Superplasticiser	1.3	1.3	1.3	1.3	1.3
Fibre (Dramix RC 65/35)	0	20	40	80	80

Table 1. Concrete mix composition

pouring. The concrete from the beginning of each batch ( $\approx 200$  l) was discarded.

It was found that for the fourth mix, with 80 kg/m<sup>3</sup> steel fibres added, there was a large scatter between the three washout samples. Consequently, a second batch was cast with the same amount of fibres (Table 2). Both batches with a fibre content of 80 kg/m<sup>3</sup> were used for further testing, and are referred to as series 1.0a and 1.0b. The five series are named according to nominal (added) fibre content as shown in Table 1.

### Material properties

For each mix, the compressive strength  $f_{cm,28d}$  and the elastic modulus  $E_{cm}$  were tested on cylinders of diameter 150 mm and height 300 mm. The compressive strength was tested according to the Swedish standard SS-EN 12390-3: 2009 (SIS, 2009) and the elastic modulus according to SS-137232: 2005 (SIS, 2005b). The splitting tensile strength  $f_{ctm,sp,28d}$  was determined after 28 days on water-cured cubes ( $150 \times 150 \times 150$  mm<sup>3</sup>) following the Swedish standard SS-EN 12390-6. The direct tensile strength was obtained as

$$1. \quad f_{ctm} = 0.7f_{ctm,sp,28d}$$

Series	Sample			Average: kg/m <sup>3</sup>
	1	2	3	
0.25	13	14.7	14.6	14.1 (0.18%)
0.5	33	34.5	36.0	34.5 (0.44%)
1.0a	68	74.0	93.0	77.5 (1.0%)
1.0b	65	65.0	67.5	65.8 (0.85%)

Table 2. Results from fibre washout

Table 3 shows the mean compressive strength, splitting strength, tensile strength, elastic modulus and density for each series.

The fibres used were hooked-end steel fibres (Dramix RC 65/35, Bekaert) with a tensile strength of 1100 MPa. Ribbed bars (diameter 16 mm) of Swedish quality B500BT were used as longitudinal reinforcement; the yield strength was 535 MPa and the elastic modulus was 200 GPa, both measured in tensile tests by the manufacturer.

### Test specimens

To get a good fibre distribution and avoid wall effects, the specimens were cut from larger prisms of size  $110 \times 152 \times 720 \text{ mm}^3$ . The prisms were cast horizontally (see Figure 2(a)). The specimen geometry is shown in Figure 2(b) and Figure 3. A ribbed  $\text{Ø}16 \text{ mm}$  reinforcement bar of quality B500BT was centrally placed in the square cross-section. The size was chosen so that, in the pull-out tests, strains on the concrete surface would be large enough to be measured, while splitting in the reference series (i.e. series 0-0) would be avoided as long as possible. The concrete cover was  $3\text{Ø}$  (i.e. 48 mm), resulting in a cross-section size of  $112 \times 112 \text{ mm}^2$ . The specimen height was 110 mm. The bonded length was 60 mm and the unbonded part was achieved by enclosing the reinforcement bar in a plastic tube. For all specimens the aim was to keep the same configuration of the ribs of the rebar, so that exactly the same number of ribs would be covered with concrete and the rebar would be faced in such a way that the ribbed sides had the same orientation in each specimen. The relative rib area  $f_R$  was calculated according to model code 90 (CEB-FIP, 1993) as

$$2. \quad f_R = \gamma h_s c_s \approx 0.065$$

where  $\gamma = 0.5$  (common value),  $h_s$  is the maximum transverse rib height and  $c_s$  is the transverse rib spacing.

For each series, five pull-out specimens (total 25) were tested in the laboratory of Structural Engineering at Chalmers University of Technology, Göteborg, Sweden.

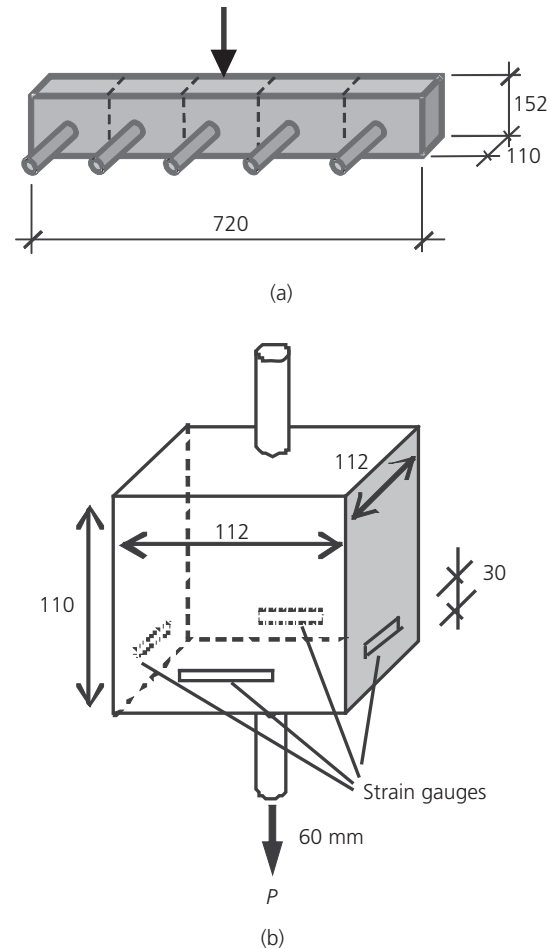


Figure 2. (a) Casting direction and geometry of the larger specimen from which test specimens were cut. (b) Geometry of the test specimens. Dimensions in mm

### Test performance

The test specimens were supported by a steel frame along the edges of the supported side. To eliminate friction, a layer of Teflon was placed between the support and the specimen (Figure 3(a)).

To monitor the displacements of the reinforcement bar, four linear variable displacement transducers (LVDT) were placed at

Series	$\frac{f_{ccm,28d}}{f_{ccm,95d}}$ : MPa	$f_{ctm,sp,28d}$ : MPa	$\frac{f_{ctm,28d}}{f_{ctm,95d}}$ : MPa	$\frac{E_{cm,28d}}{E_{cm,95d}}$ : GPa	Density: $\text{kg/m}^3$
0-0	59/65	4.1	2.9/3.1	31/33	2330
0-25	59/64	3.9	2.7/2.9	29/31	2320
0-5	58/63	4.3	3.0/3.2	31/33	2360
1-0a	59/65	4.8	3.4/3.6	31/32	2390
1-0b	50/55	4.3	3.0/3.2	30/32	2370

Table 3. Concrete properties at age 28 days and at the time of testing, 95 days

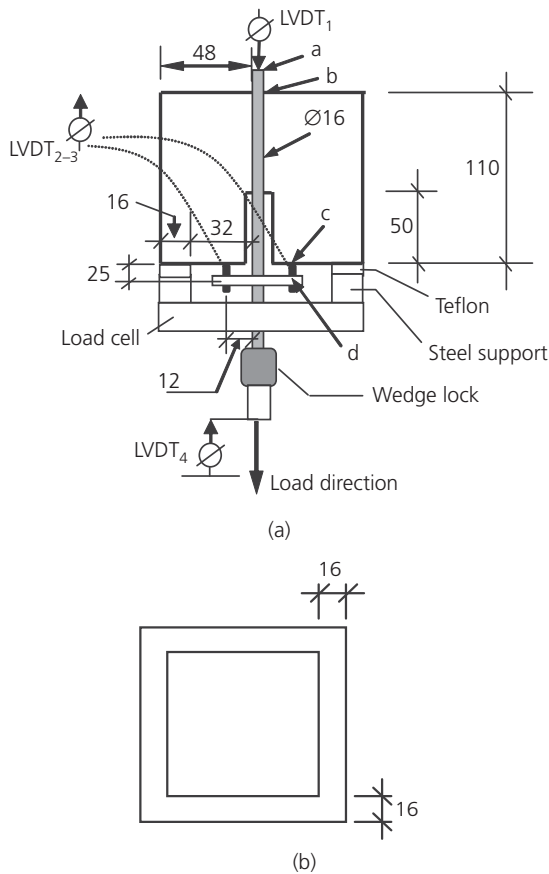


Figure 3. (a) Schematic view of test set-up. (b) Bottom view of steel support. Dimensions in mm

three different locations – one each at the top and bottom of the rebar and another two attached to the rebar just below the test specimen, as shown in Figure 3(a). LVDT<sub>1</sub> measured the displacement between points a and b (upper end of rebar and top concrete surface) and the results were used for the residual part of the bond stress–slip curves. LVDT<sub>2</sub> and LVDT<sub>3</sub> were mounted on the rebar 25 mm below the bottom concrete surface and measured the displacement between points c and d. LVDT<sub>4</sub> measured the displacement between the bottom of the grip and the machine, including sliding of the wedge lock. This gauge was used only to monitor the loading rate. The deformation was applied at a rate of approximately 0.15 mm/min. The data logging frequency was once every 5 s.

The location of the two LVDTs just below the test specimen (LVDT<sub>2,3</sub>) is considered the most appropriate place to measure. Since the aim was to study the cracking process at the beginning of loading, the displacement at this location needed to be accurate. The choice of measuring gauges for this location was therefore LVDTs with a short measuring range, which gives more precise measurements in the lower measuring range. The measuring range for LVDT<sub>2,3</sub> was ±1.000 mm, with an accuracy of 0.001 mm.

In order to investigate the ring/splitting forces, strain gauges were applied on each of the outer sides of the specimens (four gauges in series connection for each test specimen). As the largest aggregate size was 16 mm, strain gauges of length 60 mm were used.

### Finite-element analysis

The general software Diana was used for the FE analyses and the cracking behaviour was modelled using the smeared crack model based on total strain and rotating cracks (TNO, 2011). To be able to investigate splitting stresses at the interface between the matrix and the rebar, a bond model developed by Lundgren (2005) was calibrated with the experimental results.

### FE model

The FE analyses were based on a full 3D model, using tetrahedral mesh elements of base 6.2 mm and height 10.0 mm (Figure 4(c)). Figure 4(a) shows an overview of the meshed model with boundary conditions. To prevent the matrix from rotating around the rebar, four of the concrete nodes connected to the interface at the passive side were restricted in movement (Figure 4(b)). Since the edge geometry is not symmetrical relative to the grid chosen, there were no nodes located on the symmetry *x*- and *y*-axes, thus the nodal movement was restricted perpendicular to assumed symmetry lines.

### Constitutive relations

The compressive behaviour of the concrete was assumed as suggested by Thorenfeldt, following the work of Popovics (1973). For each series, the tensile softening behaviour ( $\sigma$ – $w$  relation) of the concrete was obtained experimentally by conducting uniaxial tensile testing (UTT) on notched cylinders of height  $H_c = 100$  mm and diameter  $d = 100$  mm; the depth of the notch at the mid-section was 10 mm. The average  $\sigma$ – $w$  relations for all series are shown in Figure 5.

The  $\sigma$ – $\varepsilon$  relations needed for the smeared crack model were obtained from the  $\sigma$ – $w$  relations by smearing out the crack  $w$  over a distance  $h$  (the crack-band width). A multi-linear approach (TNO, 2005) was used. The strains for the FE analyses were obtained as

$$3. \quad \varepsilon_i = \frac{f_t}{E} + \frac{w_i}{h}$$

where  $f_t$  is the tensile strength,  $w_i$  is the measured crack width from the UTT at different load stages and  $h$  is the crack-band width. The crack-band width is generally chosen as the width of one element row, with the assumption that the cracks will localise within these elements. This was observed for series 0.0 and 0.25, while for the SCSFRC with higher fibre content it was noted that the cracks did not seem to localise within this area. This is due to the nature of fibre reinforcement – after cracking, large stresses are still transferred across the crack into the

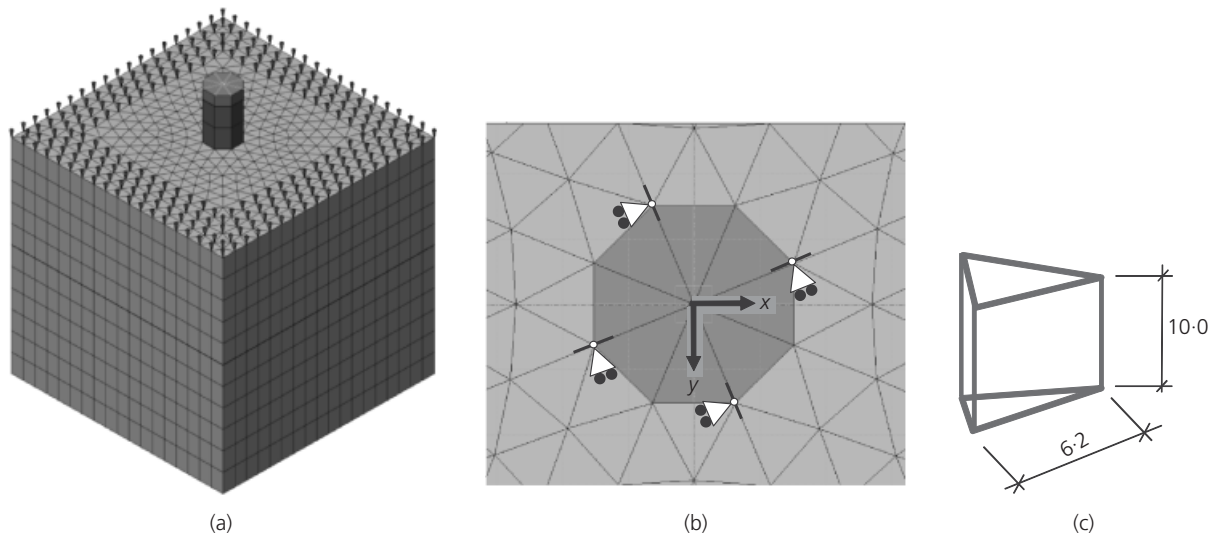


**Figure 4.** The 3D model: (a) mesh and boundary conditions; (b) supports to prevent rotation around the rebar; (c) geometry of a mesh element (dimensions in mm)

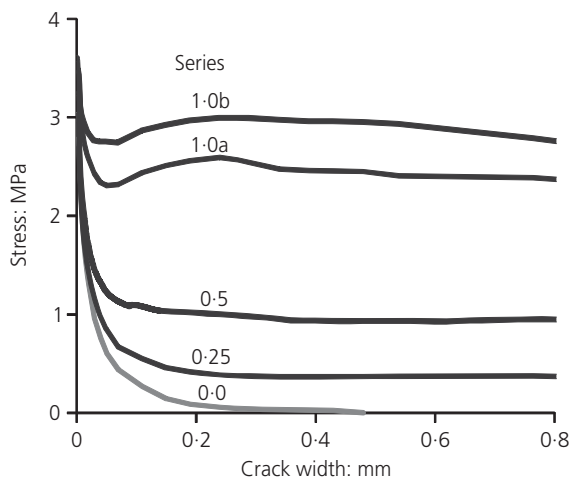


**Figure 5.** Average  $\sigma$ - $w$  curves for each series, initial part

elements adjacent to the actual crack and thus those elements may still be subjected to large strains. Choosing a larger value for  $h$  means that the dissipated energy in the analyses will decrease. The  $\sigma$ - $w$  relationship shown in Figure 5, however, indicates that the stress in the fibre concrete stays almost constant up to  $w = 0.8$  mm. For series 1.0a and 1.0b, the high residual stress-transferring capacity will not be meaningfully affected by using a larger value of  $h$  and, since the difference between peak stress and residual stress up to  $w = 0.8$  mm is quite small, the cracked elements do not lose sufficient capacity for surrounding elements to be unloaded. This is mainly due to the assumption of a homogeneous distribution of material

properties. To model cracking in concrete with high fibre volumes in a more realistic way, the microscale probably needs to be modelled. Then a fibre could be looked upon as a rebar anchored in plain concrete and the concrete surrounding it may crack. However, owing to time limitations, this was not done in the present study. Thus, for all the analyses in this study, the adopted crack-band width was  $h = 6.2$  mm, which corresponds to the mesh-element width. This choice proved to yield results in good agreement with the bond stress-slip curves obtained from the experiments.

#### Bond model

The bond model used was developed by Lundgren (2005). The model is capable of describing both the bond stress traction  $t_t$  and slip  $u_t$  along the rebar and the normal traction  $t_n$  and corresponding normal displacement  $u_n$  at the interface layer; see Figure 6(a).

The model is a frictional model, using elasto-plastic theory to describe the relations between the stresses and the deformations. Equations 4–8 are taken from Lundgren (2005). The relation between the traction  $\mathbf{t}$  and the relative displacement  $\mathbf{u}$  in the elastic range is

$$4. \quad \begin{bmatrix} t_n \\ t_t \\ t_r \end{bmatrix} = \begin{bmatrix} D_{11} & 0 & 0 \\ 0 & D_{22} & 0 \\ 0 & 0 & D_{33} \end{bmatrix} \begin{bmatrix} u_n \\ u_t \\ u_r \end{bmatrix}$$

where  $D_{22}$  and  $D_{11}$  are the tangential and normal stiffness of the interface respectively and  $D_{33}$  is a dummy stiffness added to prevent rotation of the rebar around its axis. Furthermore, the model has yield lines, flow rules and hardening laws. The traction

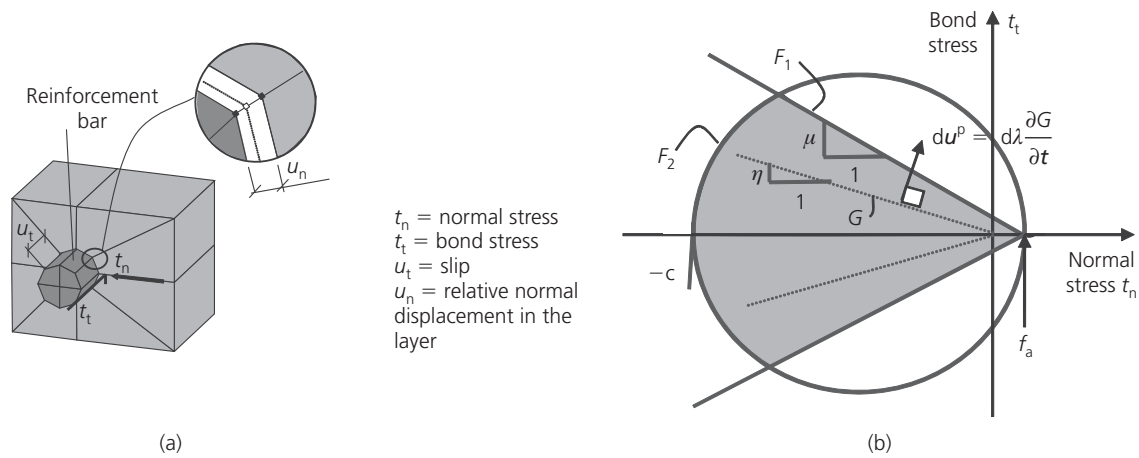


**Figure 6.** (a) Physical interpretation of variables  $t_n$ ,  $t_t$ ,  $u_n$  and  $u_t$ . (b) Yield lines  $F_1$  and  $F_2$ ; the stress in the inclined compressive struts  $c(\kappa)$  determines the upper limit at pull-out failure ( $F_2$ ) (modified from Lundgren (2005))

$t_t$  is related to the displacement  $u_t$  and has no influence on the yield lines, which are described by two yield functions. One describes the friction  $F_1$

$$5. \quad F_1 = |t_t| + \mu(t_n - f_a) = 0$$

in which  $\mu$  is the friction and  $f_a$  is the adhesion in the interface layer. The other yield line,  $F_2$ , describes the upper limit at pull-out failure. This is determined from the stress in the inclined compressive struts,  $c(\kappa)$ , which results from the bond action.

$$6. \quad F_2 = t_t^2 + (t_n + c)(t_n - f_a) = 0$$

The yield lines are shown in Figure 6(b). For plastic loading along the yield line describing the upper limit  $F_2$ , an associated flow rule is assumed. For the yield line describing the friction  $F_1$ , a non-associated flow rule is assumed, where the plastic part of the deformations is given by

$$7. \quad \begin{aligned} du^p &= d\lambda \frac{\partial G}{\partial \mathbf{t}} \\ G &= \frac{|u_t|}{u_t} t_t + \eta t_n = 0 \end{aligned}$$

in which  $d\lambda$  is the incremental plastic multiplier and  $\eta$  is the dilation parameter.

For the hardening rule of the model, a hardening parameter  $\kappa$  is established, defined as

$$8. \quad d\kappa = \left( du_n^{p2} + du_t^{p2} \right)^{1/2}$$

For monotonic loading,  $du_n^p$  and the elastic part of the slip are very small compared to the plastic part of the slip  $du_t^p$ ; therefore the hardening parameter  $\kappa$  will be almost equivalent to the slip  $u_t$ . The variables  $\mu$ ,  $f_a$  and  $c$  in the yield functions are assumed to be functions of  $\kappa$ .

#### Input parameters for the interface

Required input data for the interface are the elastic stiffness matrix  $\mathbf{D}$  in Equation 4, the dilatation parameter  $\eta$  defined in Equation 7 and, for loading in the damaged deformation zone, parameters  $\eta_{d0}$  and  $\mu_{d0}$ , as shown in Table 5. Furthermore, the functions  $c(\kappa)$ ,  $\mu(\kappa)$  and  $f_a(\kappa)$  must be chosen, as discussed later.

#### Comparison of experimental and numerical results

##### Experimental results

The average ascending part of the curves is shown in Figure 7. Up to peak, the results were plotted against the slip measured on the active side; for the residual part, the slip measured on the passive side was used. In the FE model, the displacement was extracted at the location where LVDT<sub>2</sub> and LVDT<sub>3</sub> were placed on the test specimen; therefore, the displacement measured at this location in the experiments was not adjusted regarding the elastic elongation of the rebar. For comparison with CEB-FIP model code 2010 (CEB-FIP, 2010), only the slip on the passive side (LVDT<sub>1</sub>) was used.

Table 4 shows the average maximum bond stress for each series. The series with the lowest compressive strength (series 1-0b) exhibits the lowest stiffness as well as the lowest maximum value. As mentioned, this series showed the lowest compressive strength,

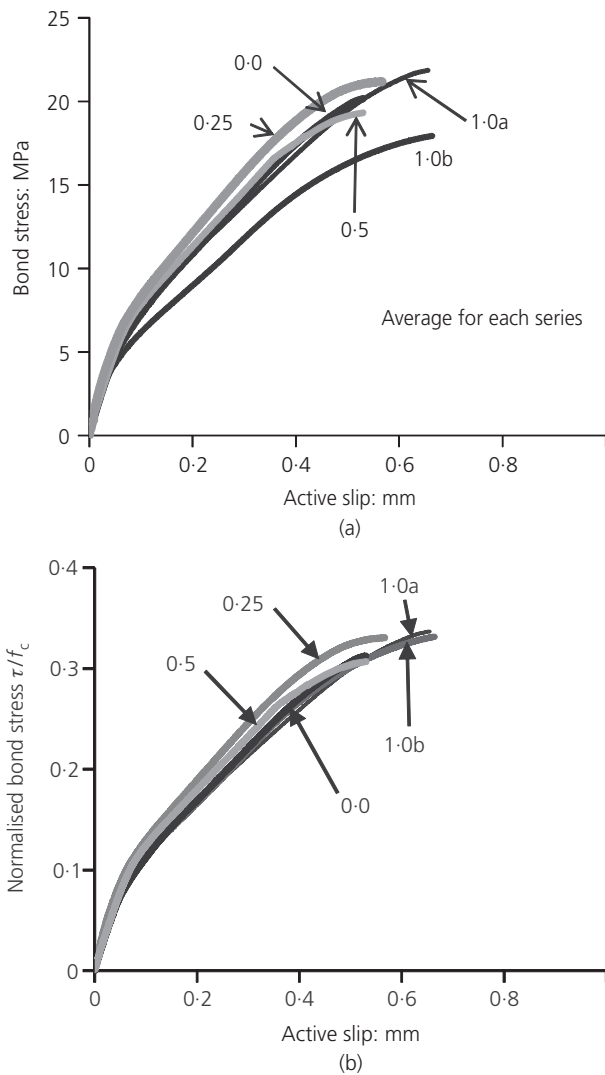


**Figure 7.** Bond stress–slip: (a) comparison of the average ascending branch for each series; (b) as (a) but normalised with compressive strength

$f_{cm,95d} = 55$  MPa compared with 63–65 MPa for the other series. When normalising the bond stress with the compressive strength as suggested by Magnusson (2000), Figure 7(b) shows that all the series show nearly identical initial stiffness and capacity.

### Experiments and numerical analyses

The bond model was originally calibrated for normal-strength concrete without fibres (vibrated) and rebar K500ST with a diameter of 16 mm. Figure 8 shows the result from using the originally suggested input for series 0.5, where it can be seen that the initial stiffness is too low and the peak and residual stresses are unacceptably high. It should be noted that the main focus of the original calibration was anchorage failure (Lundgren, 2005) and thus larger slip values than considered here were of interest. This is probably the main reason for the need of change in calibration, even though some part of it can be attributed to the change from normal vibrated concrete to SCC.

To fit the experimental results from the SCSFRC, the original input had to be changed. First, according to the reasons discussed above, the initially recommended values of the stiffnesses  $D_{11}$  and  $D_{22}$  were increased by approximately factors 2 and 5 respectively in order to fit the initial stiff behaviour of the experimental bond–slip curves (Equations 9 and 10).

$$9. \quad D_{22} = K_{22} E_c$$

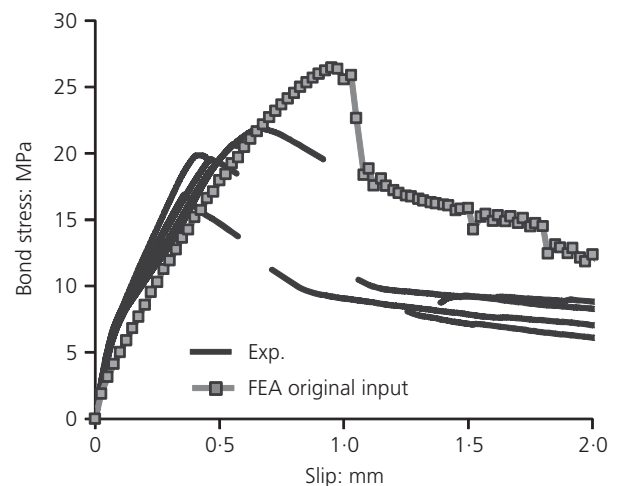


**Figure 8.** FE results for series 0.5 when using the originally suggested input

	Series				
	0.0	0.25	0.5	1.0a	1.0b
Average	20.9	22.1	19.9	22.5	19.1
Max/min	21.4/20.3	23.5/19.9	22.2/17.0	24.5/20.1	20.3/18.0

**Table 4.** Bond strength for each series

10.  $D_{11} = 9.5D_{22}$

11.  $D_{33} = 1E_{11}$

with  $K_{22} = 35 \text{ m}^{-1}$  and  $E_c$  in Pa,  $D_{22}$  is obtained in  $\text{N/m}^3$ .

To determine the most appropriate input for  $\eta$ ,  $\mu(\kappa)$  and the adhesion  $f_a(\kappa)$ , different values were combined until the FE results showed acceptable agreement with the experiments.

It seems reasonable to start by assuming that the actual interface zone stays unaffected by the fibre reinforcement used here; hence it should be possible to use the same input for all the series. Figure 9 shows the FE results for all series when the input listed in Table 5 was used; the FE results well resemble the experimental trend regarding both initial stiffness and stress magnitudes. Figure 10 shows comparisons between FE results and experiments for the individual bond stress–slip curves.

Figure 10 shows that the input in Table 5 worked well for series 0.0, 0.25 and 0.5 regarding initial stiffness, peak and residual stress. Series 0.0 failed in splitting, both in tests and in analyses. Series 0.25 and 0.5, on the other hand, showed splitting behaviour but kept some confinement due to the fibre reinforcement, again both in the tests and analyses. Series 1.0a showed good agreement regarding initial stiffness and peak stress, while for series

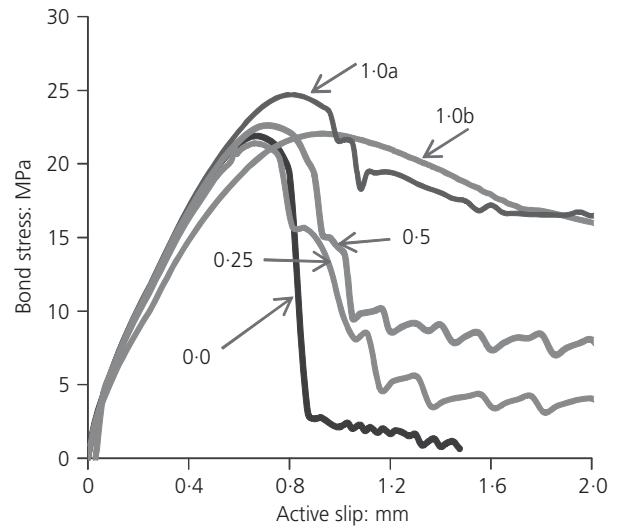


Figure 9. Comparison of FE results from all the series using the input shown in Table 5

1.0b the peak stress in the analysis was about 10% higher than the highest stress in any of the tested specimens. Both series with the highest fibre content (series 1.0a and 1.0b) exhibited pull-out failure both in tests and in analyses.

Parameter study

Strength of the inclined compressive struts  $c(\kappa)$

As the slip of the rebar increases, the concrete close to the ribs becomes compressed and eventually the material strength

DSTIF	$D_{11} = 9.5D_{22}$	$D_{22} = K_{22}E_c$	
User values			
$D_{12}$	$\mu_{d0}$	$\eta$	$\eta_{d0}$
$\kappa$ : mm	$c(\kappa)$ : Pa	$\mu(\kappa)$	$f_a(\kappa)$ : Pa
0	$f_c$	1.00	$f_{ct}$
0.135	$1.000f_c$	0.86	$10^{-4}f_{ct}$
0.280	$0.997f_c$	0.78	0
0.411	$0.992f_c$	0.72	0
0.621	$0.964f_c$	0.65	0
0.830	$0.939f_c$	0.59	0
1.070	$0.870f_c$	0.56	0
1.510	$0.757f_c$	0.52	0
1.900	$0.704f_c$	0.52	0
2.600	$0.642f_c$	0.52	0
4.710	$0.541f_c$	0.52	0
12.100	$0.676f_c$	0.52	0
$1.50 \times 10^{20}$	0	0.52	0

Table 5. Input for the parameters used in the bond model

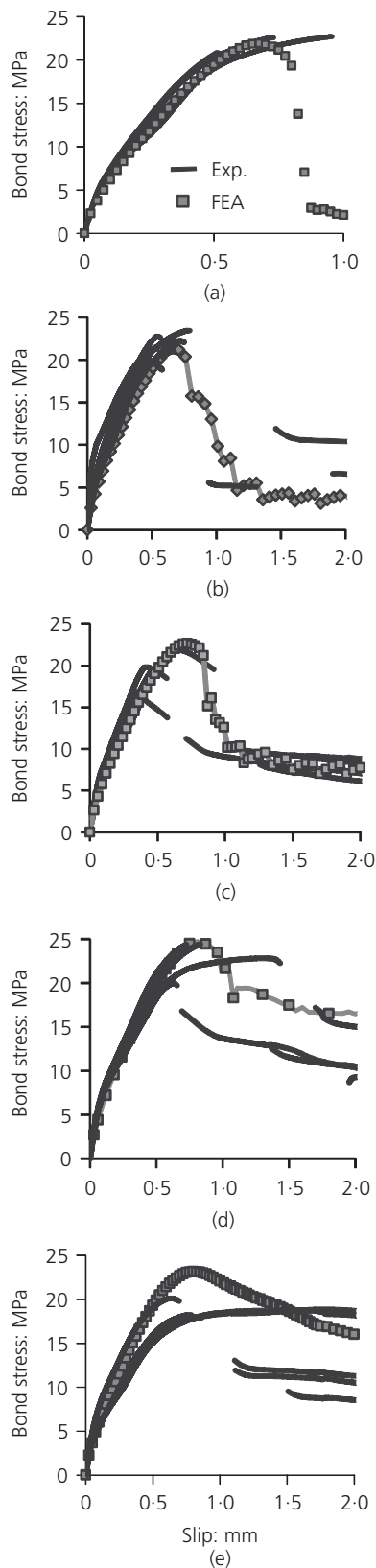


Figure 10. Comparison of FE results using the input shown in Table 5 with experiments for series: (a) 0.0, (b) 0.25, (c) 0.5, (d) 1.0a and (e) 1.0b

decreases. When using the original input for  $c(\kappa)$ , the residual stress was overestimated for series 1.0a and 1.0b with the highest fibre content. The reason for this can probably be explained as follows. When the peak stress is reached (which was about the same for all series), the normal stresses quickly deteriorate for the cases exhibiting splitting failure. This means that the confinement is reduced, or lost, and the strength of the inclined compressive struts,  $c(\kappa)$ , has little or no effect on the remaining part of the analysis. For pull-out failure, on the other hand, the confinement is kept intact or with only slight damage; thus the normal stresses do not deteriorate. In this case,  $c(\kappa)$  must decrease properly or else the bond stress will not decrease as expected for increased slip. Figure 11(a) shows the original and calibrated inputs for series 1.0b and Figure 11(b) shows the effect of the two inputs. It can be

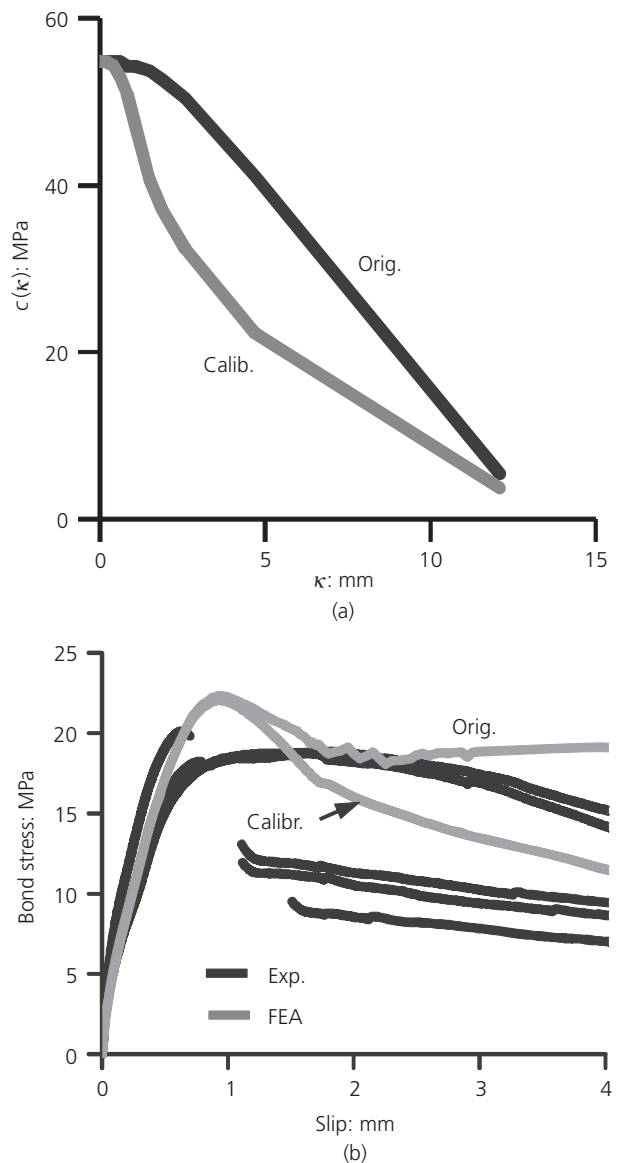


Figure 11. (a) Calibrated  $c(\kappa)$  and (b) effect of using the calibrated values for series 1.0b

seen that with the calibrated input, the decrease in residual stress showed better agreement with the experiments.

### Adhesion $f_a$

At the very beginning of the pull-out action of the rebar, the adhesion acts together with the friction in resisting the slip. The adhesion strength was not measured; physically, though, it seems natural to let the adhesion be limited by the tensile strength of the matrix. This was also assumed by Bolmsvik and Lundgren (2006). The results from the analyses tended to agree best with the experimental results when the adhesion was set equal to the matrix tensile strength and approached zero for a quite small movement of the rebar, at  $\kappa = 0.135$  mm (see Table 6). The analyses showed that small variations in the maximum adhesion value did not affect the result. If it was left active past  $\kappa = 0.135$  mm, the bond stiffness was marginally increased. Figure 12(a) shows the effect of letting the adhesion be active for three different ranges of the hardening parameter  $\kappa$ . As can be seen, the effect is small.

It was found that for all the series, alternative B (Table 6) for  $f_a$  was the one that gave best agreement with the experiments. This also agrees with reality, since the nature of adhesion is chemical bonding and is lost for deformations already in the micrometre range (Dupont, 2003).

### Friction

Friction depends on the geometry and spacing of the ribs on the rebar as well as on the properties of the interface layer between the rebar and matrix. The increased amount of fine particles (powder) in a SCC matrix most likely results in a stiffer ascending branch of the bond stress–slip curve, as seen in the experiments. This can be attributed to the higher packing grade of SCC compared with vibrated concrete. It is also possible that it can lead to improved friction (regarding both fibres and rebar) since the fine particles more easily fill out the spaces in the interface zone. Furthermore, Banthia *et al.* (1993) found that the peak bond stress was increased in SCC.

Theoretically, there is the possibility of a negative effect due to fibre reinforcement, with fibres blocking the finest aggregates/cement paste so that voids are created in the interface zone; for

$\kappa$ : mm	$\mu$	$f_a$		
		A	B	C
0	1.0	0	$f_{ct}$	$f_{ct}$
0.135	0.86	0	$10^{-4}f_{ct}$	$f_{ct}$
0.280	0.78	0	0	$10^{-4}f_{ct}$
0.411	0.72	0	0	0

Table 6. Different inputs for  $f_a(\kappa)$

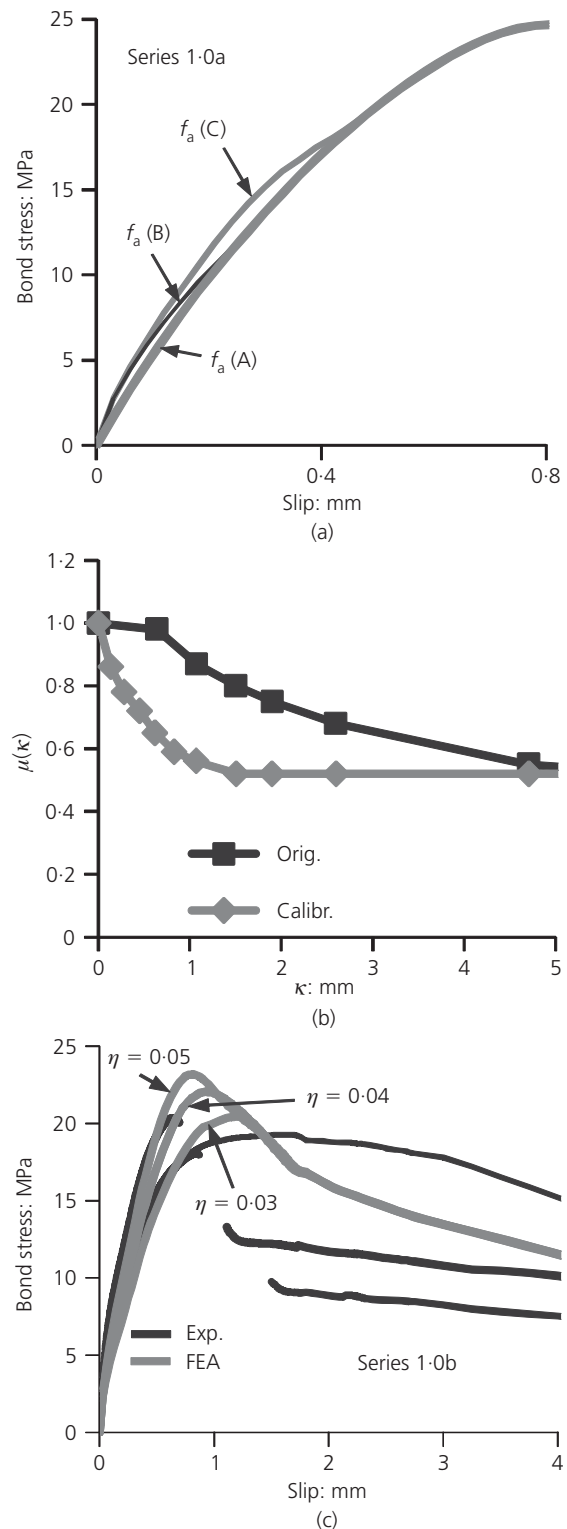


Figure 12. (a) Effect of adhesion  $f_a$  on bond stress, with the input listed in Table 6. (b) Original  $\mu(\kappa)$  and calibrated  $\mu(\kappa)$  used in the analyses. (c) Effect of  $\eta$  on the bond stress–slip curve, shown here for series 1-0b

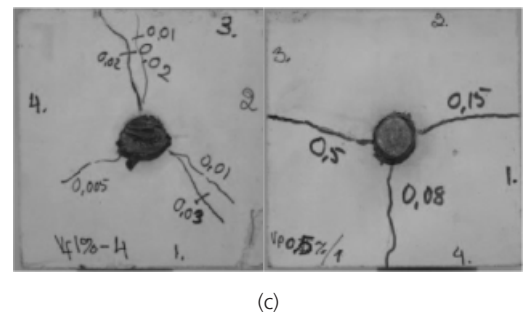
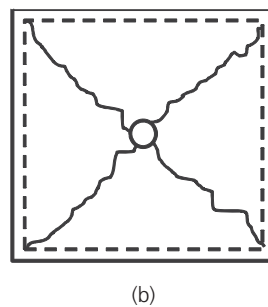
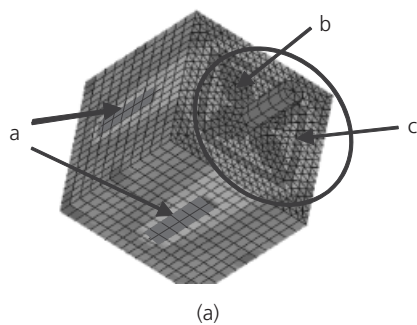
example, Grünewald (2004) found that fibres decrease the packing grade in SCC. Fibre-reinforced concrete needs more cement paste and this was considered in the manufacture of the concrete tested in this work. Therefore, a lower packing grade seems not to have been the case in the tests reported here.

Figure 12(b) shows the calibrated  $\mu(\kappa)$  used in the analyses together with the original suggestion. The results indicate that the reason for the new lower calibration could be that SCC, with its higher packing grade, gives an initially stiffer behaviour. Due to its higher brittleness, though, friction is lost more quickly than for the vibrated concrete originally used.

In the bond model used, the values for  $\mu(\kappa)$  are chosen independently of the normal displacement  $u_n$ . Equation 8 shows that  $u_n^p$  is a parameter of the function  $\kappa$  and thus the coefficient of friction will depend on the plastic part of the normal displacement. However, this is very small compared with the plastic part of the slip ( $u_t^p$ ) and therefore, in practice, the normal displacement will have no effect on the frictional values in the model. In reality, the friction will decrease when the normal deformation between the matrix and the rebar increases. One way to obtain that in the model would be to introduce a factor by which  $du_n^p$ , in Equation 8, would be multiplied. This will be left for future analyses.

#### Dilatation parameter $\eta$

The dilatation parameter  $\eta$  has a large impact on the analysis results. It affects the interface movement in the normal direction and, the larger  $\eta$  is, the more the two interface surfaces want to separate. Thus, for a larger  $\eta$ , the peak load will be reached for a smaller slip value. In the experiments it was seen that series 1-0b showed a lower stiffness than the other series. To capture this in the analyses, it was necessary to choose a lower value of  $\eta$ . Figure 12(c) shows a comparison between  $\eta = 0.03$ , 0.04 and 0.05. For series 1-0b, the best agreement with the experiments was found for  $\eta = 0.04$ ; for the other series, the best agreement was for  $\eta = 0.05$ .



**Figure 14.** (a) Contour plot of maximum principal strain  $\epsilon_1$  for series 1-0b. (b) Crack pattern in simply supported quadratic plate according to yield-line theory. (c) Examples of crack patterns from series 1-0a and 0-5

#### Surface strains and crack pattern

One of the benefits of FE analysis is the possibility to evaluate strains on the concrete surface. Due to the homogeneous distribution of material properties in FE analysis, the strains on all four sides are identical up to the point where the concrete cracks. This is not the case in experiments where different material properties allow for variations in the strain magnitudes between the four monitored surfaces. The surface strains in the FE analyses agreed well with the experiments; see Figure 13 for an example.

Figure 14(a) shows the main principal strain  $\epsilon_1$  in series 1-0b. Cracking starts as two separate actions

- (a) one originating from the stresses induced by the inclined compressive struts
- (b) one resulting from the edge supports on the active side.

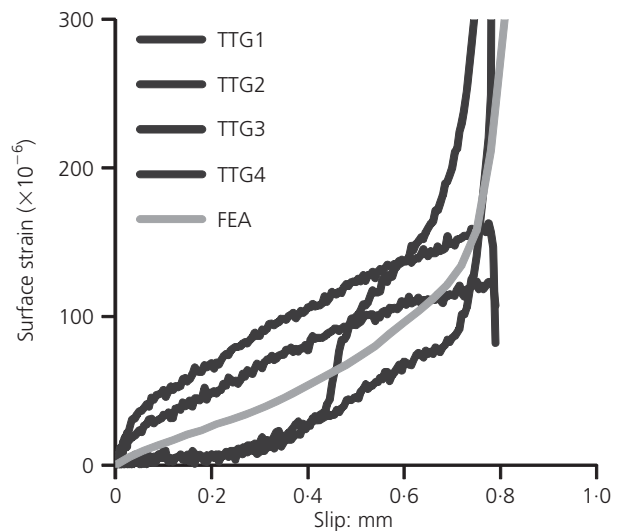


**Figure 13.** Example of surface strains in series 1-0b compared with the measured strain on each of the four sides in one of the test specimens (TTG1–4 refer to respective strain gauges)

Furthermore, it is seen in the analyses that the initial crack pattern on the active side resembles the envelope-looking crack pattern found in a simply supported plate/slab described with yield-line theory. The concentration of strains in the model (area  $b$  in Figure 14(a)) corresponds with the yield lines shown in Figure 14(b). For further loading (just before and beyond peak), the cracks arising from action ( $a$ ) will dominate in the analyses. This is due to the homogeneous distribution of the material properties, which allows the shortest distance to the surface to dictate the final behaviour. The random distribution of material properties in the experiments most likely explains why some cracks keep developing diagonally even though this is the longest distance between the rebar and the concrete surface (Figure 14(c)).

### Comparison of results with model code 2010

Hamad *et al.* (2011) investigated the effects of fibre reinforcement on the bond performance of hooked bars anchored in normal-strength concrete beam–column connections. They also discussed earlier research by several authors regarding the effects of fibre reinforcement on improving the bond behaviour in different anchoring situations. All comparisons were made with concrete without transverse reinforcement and it was found that steel fibres effectively change the failure mode from brittle to ductile splitting. However, different conclusions were reached regarding the maximum bond strength.

As fibre reinforcement is able to partly or completely replace stirrups, it is of interest to compare its confining ability with that of stirrups. Model code 2010 (CEB-FIP, 2010) presents a model for the case of splitting with stirrups for good bond conditions; the confining effect of the stirrups depends on the ratio  $K_{tr}$

$$12. \quad K_{tr} = \frac{n_1 A_{sv}}{n_b \phi S_v}$$

where  $n_1$ ,  $A_{sv}$  and  $S_v$  are number of legs, cross-sectional area of one leg and spacing of the confining reinforcement respectively,  $n_b$  is the number of anchored bars and  $\phi$  is the diameter of the anchored bar.  $K_{tr}$  may be viewed as a ratio defining how much confining reinforcement there is per anchored bar. This model was used to estimate the amount of transverse reinforcement to which the fibres corresponded. Thus, the input was, as in the experiments, a 16 mm diameter rebar anchored in a square cross-section ( $112 \times 112 \text{ mm}^2$ ) with corresponding compressive strength (i.e.  $f_{cm,95d}$ ) as listed in Table 3. The amount of transverse reinforcement was varied until a reasonable agreement with the experimental residual capacity was found (Figure 15). For each series, Table 7 lists the amount of stirrups needed (in terms of diameter  $\phi$  and spacing  $S_v$ ), together with corresponding values of  $K_{tr}$ , to obtain a confinement after cracking that is comparable with that of the fibre reinforcement. The experimental results in Figure 15 are plotted against the slip measured solely on the passive side.

Model code 2010 mentions that the proposed bond model should be considered a statistical mean for a broad range of cases and that further reliability handling is needed to obtain design bond stress–slip relationships. Figure 15 shows a comparison of the bond stress–slip curves from the experiments with two cases suggested by the model code: a confined situation and splitting with stirrups. It is worth noting that, for large amounts of transverse reinforcement, the capacity for splitting with stirrups becomes larger than for the confined situation; this is questionable and it would be reasonable to limit the splitting bond stress to the maximum bond stress for the confined condition.

Although series 1·0a and 1·0b showed pull-out failure and thereby ought to be best represented by the case with confined model and good bond conditions in model code 2010, the case of splitting with stirrups was also considered in order to obtain an estimate of the amount of stirrups that would yield the same confinement as the fibre reinforcement in these two series. It can be seen that the peak stress and the stiffness before peak, for SCSFRC material, are underestimated by the proposed model. Magnusson (2000) experienced the same when comparing experimental results for high-strength concrete with model code 90 (CEB-FIP, 1993). Figure 15 shows that the peak stress, in the SCSFRC material tested here, is better described by the confined model with good bond conditions. Possibly the stiffness of the ascending branch, and the maximum bond stress, should also depend on the type of concrete (e.g. high-strength or self-compacting).

### Additional comments

The bond model used was found to be capable of describing all the phenomena found in the experiments. In addition, it was possible to study stress development inside the specimens. It is well worth noting that, judging from the results of the tests reported in this paper, the fibre reinforcement neither disturbed nor improved the bond properties at the interface layer. The effect of adding fibres could instead be seen in the markedly increased residual capacity due to the extra confinement provided by the fibres. This is a valuable gain since, for example, it could enable the use of fibre reinforcement as a replacement for stirrups in an anchorage zone. With more experimental data, the model in CEB-FIP model code 2010 could probably be developed to include the effect of fibre reinforcement.

### Conclusions

There are contradictory reports regarding the effect of fibre reinforcement on bond in the literature. This paper reports on pull-out tests with short embedment length using self-compacting steel-fibre-reinforced concrete and FE analyses of the results. Based on this work the following conclusions may be drawn.

- (a) The fibre reinforcement did not disturb or improve the bond properties at the interface layer. Thus, the pre-peak behaviour seems to be unaffected by the inclusion of steel fibres.
- (b) Compared with the original calibration for vibrated concrete, an initially stiffer bond stress–slip behaviour was found; SCC

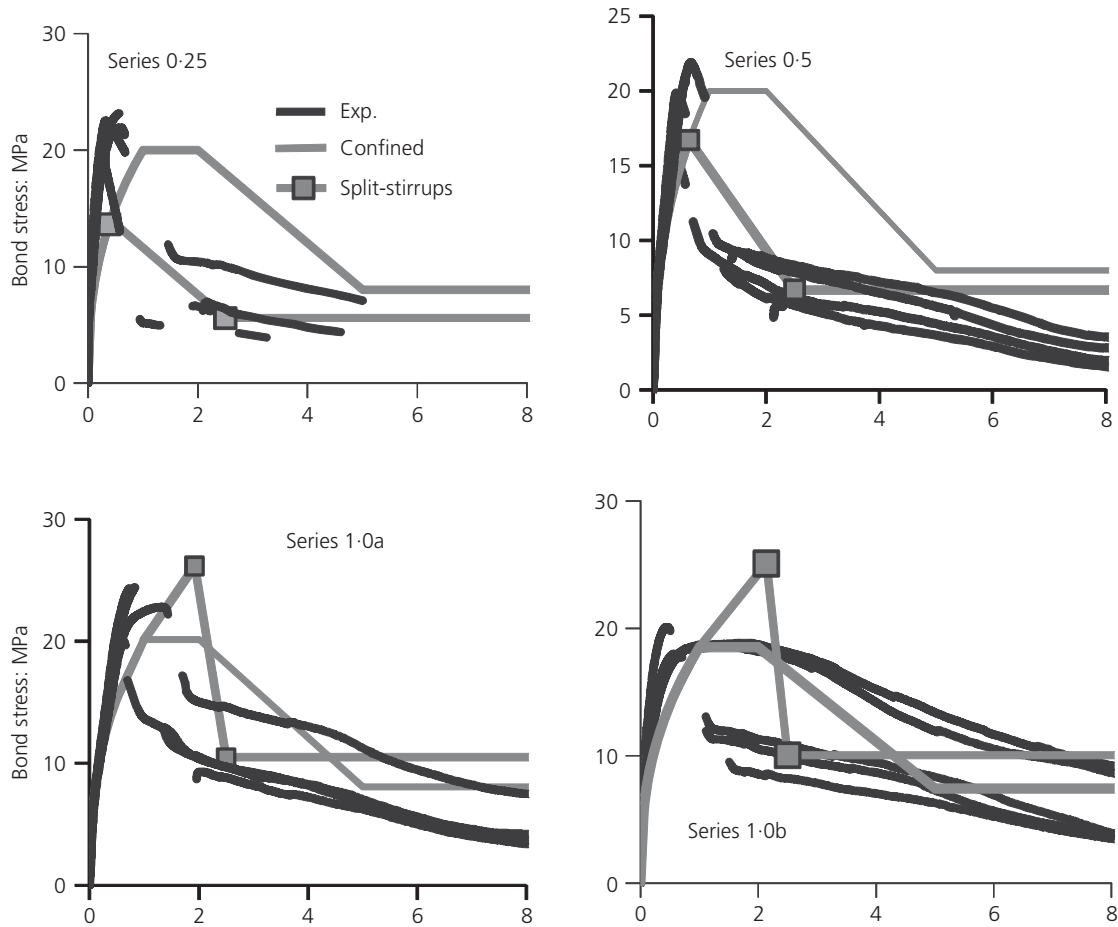


**Figure 15.** Comparison of the confining ability of each series with the bond model proposed in CEB-FIP model code 2010 (CEB-FIP, 2010)

Series	$\phi$ : mm	$S_v$ : mm	$K_{tr}$ : %
0-25	6	300	1.2
0-5	10	200	4.9
1-0a	12	80	18
1-0b	12	80	18

**Table 7.** Diameter and spacing of stirrups and corresponding ratio  $K_{tr}$  needed to obtain confinement comparable with fibre reinforcement

thus appears to improve the local concrete–fibre and concrete–rebar bonds.

- (c) The confinement was markedly improved by the addition of fibre, resulting in an increasing residual capacity for an increasing amount of fibre reinforcement.
- (d) When comparing the confinement effect with the bond model proposed in model code 2010 (CEB-FIP, 2010) it was found

that, for series 0-25 and series 0-5, the fibres corresponded to 1.2% and 4.9% confining reinforcement respectively. For series 1-0a and 1-0b, the fibre reinforcement corresponded closely to confined conditions.

- (e) Cracking was found to arise from two separate actions – one giving rise to diagonal cracks on the supported active side and the other originating from the tensile stresses induced by the inclined compressive struts from the bond mechanism.
- (f) The crack patterns from the analyses were in good agreement with those observed experimentally and the surface strains were also well captured.
- (g) The failure modes were well captured by the FE analyses.

#### REFERENCES

- Banthia N, Azzabi M and Pigeon M (1993) Restrained shrinkage cracking in fibre-reinforced cementitious composites. *Materials and Structures* **26**(7): 405–413.
- Bigaj-van Vliet AJ (2001) *Bond of Deformed Reinforcing Steel Bars Embedded in Steel Fiber Reinforced Concrete State-of-the-art Report*. Delft Cluster, Delft, Netherlands, p. 65.

- Bischoff P (2003) Tension stiffening and cracking of steel-fiber-reinforced concrete. *Journal of Materials in Civil Engineering* **15**(2): 174–182.
- Bolmsvik R and Lundgren K (2006) Modelling of bond between three-wire strands and concrete. *Magazine of Concrete Research* **58**(3): 123–133.
- CEB-FIP (1993) *Model Code 90*. CEB-FIP, Lausanne, Switzerland, Bulletin d'Information 213/214, p. 437.
- CEB-FIP (2010) *CEB-FIP Model Code 2010*, Vol. 1. International Federation for Structural Concrete (fib), Lausanne, Switzerland, Bulletin 55, First complete draft.
- Chao SH, Naaman AE and Parra-Montesinos G (2009) Bond behaviour of reinforcing bars in tensile strain-hardening fiber-reinforced cement composites. *ACI Structural Journal* **106**(6): 897–906.
- Dupont D (2003) *Modelling and Experimental Validation of the Constitutive Law ( $\sigma$ - $\epsilon$ ) and Cracking Behaviour of Steel Fibre Reinforced Concrete*. PhD thesis, Catholic University of Leuven, Leuven, Belgium.
- Grünwald S (2004) *Performance-based Design of Self-compacting Fibre Reinforced Concrete*. PhD thesis, Delft University of Technology, Delft, Netherlands.
- Hamad BS, Haidar EYA and Harajli MH (2011) Effect of steel fibers on bond strength of hooked bars in normal-strength concrete. *ACI Structural Journal* **108**(1): 42–50.
- Lundgren K (2005) Bond between ribbed bars and concrete. Part 1: modified model. *Magazine of Concrete Research* **57**(7): 371–182.
- Magnusson J (2000) *Bond and Anchorage of Ribbed Bars in High-Strength Concrete*. PhD thesis, Chalmers University of Technology, Göteborg, Sweden.
- Noghabai K (1998) *Effect of Tension Softening on the Performance of Concrete Structures: Experimental, Analytical and Computational Studies*. PhD thesis, Luleå University of Technology, Luleå, Sweden.
- Popovics S (1973) A numerical approach to the complete stress-strain curve of concrete. *Cement and Concrete Research* **3**(5): 583–589.
- SIS (Swedish Standards Institute) (2004) SS-EN 12390-6:2004: Proving av hårdnad betong – Del 6: Spräckhållfasthet hos provkroppar. SIS, Stockholm, Sweden.
- SIS (2005a) SS-EN 14721: 2005: Förtillverkade betongprodukter – Provningsmetod för betong med metallfibrer – Bestämning av fiberinnehållet i färsk och hårdnad betong. SIS, Stockholm, Sweden.
- SIS (2005b) SS-137232: 2005: Betongprovning – Hårdnad betong – Elasticitetsmodul vid tryckprovning. SIS, Stockholm, Sweden.
- SIS (2009) SS-EN 12390-3: 2009: Proving av hårdnad betong – Del 3: Tryckhållfasthet hos provkroppar. SIS, Stockholm, Sweden.
- Tepfers RA (1973) *Theory of Bond Applied to Overlapped Tensile Reinforcement Splices for Deformed Bars*. PhD thesis, Chalmers University of Technology. Göteborg, Sweden.
- TNO (2005) *DIANA – Finite Element Analysis, User's Manual Release 9.3*. TNO, Delft, Netherlands.
- TNO (2011) *DIANA – Finite Element Analysis, User's Manual Release 9.4.3*. TNO, Delft, Netherlands.
- Zhu W, Sonebi M and Bartos PJM (2004) Bond and interfacial properties of reinforcement in self-compacting concrete. *Materials and Structures* **37**(7): 442–448.

---

#### WHAT DO YOU THINK?

To discuss this paper, please submit up to 500 words to the editor at [www.editorialmanager.com/macr](http://www.editorialmanager.com/macr) by 1 January 2013. Your contribution will be forwarded to the author(s) for a reply and, if considered appropriate by the editorial panel, will be published as a discussion in a future issue of the journal.